MambaEye: A Size-Agnostic Visual Encoder with Causal Sequential Processing

Changho Choi Korea University

changho98@korea.ac.kr

Minho Kim MIT

lgmkim@mit.edu

Jinkyu Kim Korea University

jinkyukim@korea.ac.kr

Abstract

Despite decades of progress, a truly input-size agnostic visual encoder—a fundamental characteristic of human vision—has remained elusive. We address this limitation by proposing MambaEye, a novel, causal sequential encoder that leverages the low complexity and causal-process based pure Mamba2 backbone. Unlike previous Mamba-based vision encoders that often employ bidirectional processing, our strictly unidirectional approach preserves the inherent causality of State Space Models, enabling the model to generate a prediction at any point in its input sequence. A core innovation is our use of relative move embedding, which encodes the spatial shift between consecutive patches, providing a strong inductive bias for translation invariance and making the model inherently adaptable to arbitrary image resolutions and scanning patterns. To achieve this, we introduce a novel diffusion-inspired loss function that provides dense, step-wise supervision, training the model to build confidence as it gathers more visual evidence. We demonstrate that MambaEye exhibits robust performance across a wide range of image resolutions, especially at higher resolutions such as 1536² on the ImageNet-1K classification task. This feat is achieved while maintaining linear time and memory complexity relative to the number of patches.

1. Introduction

A central goal in computer vision is a truly *input-size ag-nostic* encoder. These encoders will ideally operate on arbitrary resolutions and allocates resources based on availability, without committing to a fixed input size. While high resolution media is becoming more common, most vision encoders are limited on their ability to work on various input dimensions. Instead, these encoders typically resize or crop during the data piping process, incurring unavoidable information loss which could be detrimental to the task.

The disadvantages from this lack of versatility is already well-known in many models but is difficult to solve. Convolutional Neural Networks (CNNs) [8, 14], while endowed

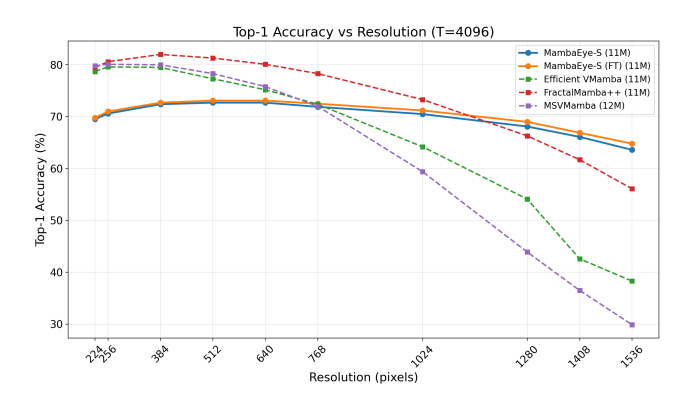


Figure 1. **MambaEye Resolution Scaling** Our MambaEye-S (11M params) models are benchmarked against Mamba-based models of similar size. While deterministic scanning methods like FractalMamba++ [15] achieve higher peak accuracy at medium resolutions, our model demonstrates superior scaling at extreme resolutions. Notably, MambaEye outperforms FractalMamba++ at resolutions over 1280², despite using only a naive random sampling policy. This highlights our architecture's inherent robustness and size-agnostic capabilities.

with strong inductive biases, rely on fixed-size kernels whose effective receptive field grows slowly with depth, making global reasoning at high resolution costly. Vision Transformers (ViTs) [5] provide global receptive fields but incur quadratic complexity in the number of patches, which rapidly becomes prohibitive for native-resolution inputs [24]. Previous remedies such as linear/sparse attention [16, 34, 38] reduce the cost at the expense of expressivity. To complicate matters, standard ViT pipelines require resizing and often overfits to the image size of the training data by learning the absolute positional embeddings. Even with sophisticated training strategies such as FixRes [32] or relative encodings (e.g., RoPE) [10, 31], the resolution brittleness persists.

State Space Models (SSMs) such as Mamba [6], offer a better chance of realizing an input-size agnostic encoder due to their linear-time scaling and constant-memory recurrent inference, making them attractive for long sequences. However, when adapted to vision, most approaches seri-

alize images with fixed, hand-crafted scanning paths [13] (e.g., raster scanning), disrupting 2D locality. Many Mamba based encoders also rely on bidirectional processing to compensate [19, 39], which forfeits the memory advantages of causal recurrence. Recent work on fractal/space-filling traversals improves locality [15, 33] but still enforces a predefined, holistic scan and does not eliminate the need to pick a fixed resolution up front.

To have a truly size-agnostic model, we can once again turn to human vision perception. A human gathers information by dynamically scanning a scene, not by processing with a certain deterministic path. From this, unlike other architectures, we emphasize the importance of causal and sequential nature of vision perception. An ideal model should see the same part of the image multiple times, without a dependence in the order they are seen. Human vision rarely concludes the scene in one shot; instead, it cumulates information through time to build a confident understanding.

With these motivations in mind, we propose Mamba-Eye, a causal and sequential visual encoder built on from pure Mamba2 backbone [3] that directly addresses these issues. Instead of committing to a global, fixed traversal or training resolution, MambaEye processes an *arbitrary* sequence of patches and can emit a prediction at any step. Two design choices enable this: (1) a **relative move embedding** that encodes the spatial displacement between consecutive patches, providing a strong inductive bias for translation invariance and making the model independent of image resolution and scan order; and (2) a **diffusion-inspired loss** [2, 11], conceptually related to flow matching [17], that provides dense, step-wise supervision by scheduling targets from a uniform prior to the ground truth according to observed information.

This design preserves the causal, recurrent nature of SSMs at inference, enabling constant memory per step and predictions at any point in the sequence.

Interestingly, this can be achieved without the need of deterministic scanning patterns. For MambaEye, random sampling is much more successful compared to more sophisticated scanning protocols such as raster scan (Table 5).

From this new paradigm, an additional point of improvement is introducing a new diffusion-inspired loss. This loss function guides the model to calibrate its confidence at any arbitrary timestep, which leads to improved generalization on longer sequences. This also incorporates the human vision perception where we cumulate information through time. Indeed, compared to the standard cross entropy loss (Table 4).

Empirically, MambaEye achieves a competitive ImageNet-1K [28] results while exhibiting robust scaling across resolutions and outperforming previous Mamba based encoders, such as FractalMamba++ [15] at larger image sizes (Figure 1).

Our primary contributions can be summarized as the following:

- 1. We propose **MambaEye**, a novel and efficient visual encoder that is size-agnostic and causal.
- We introduce a relative move embedding technique that provides translation invariance and flexibility for arbitrary scanning paths.
- We design a new diffusion-inspired loss function that provides dense, step-wise supervision for sequential encoders.

2. Related Work

2.1. Sequential and Active Vision Paradigms

Sequential processing of visual information has long been studied as a biology-inspired alternative to holistic image encoding. Early work in recurrent attention models demonstrated that neural networks could learn to selectively attend to image regions through reinforcement learning, processing high-resolution images via sequences of focused glimpses [1, 21]. This paradigm is inspired by the saccadic movements of human eyes, in that rapid shift of attention across a visual scene rather than processing all information simultaneously is how humans perceive information.

Recent advances have extended these ideas in several directions. The Continuous Thought Machine [4] explores how neural dynamics and synchronization can enable emergent reasoning capabilities, using sparse supervision at selected timesteps rather than dense feedback. Other approaches have investigated information-theoretic frameworks for modeling eye movements [26] and generative models that learn task-driven sequential processing strategies [22]. These works demonstrate that sequential visual processing can be both efficient and effective when properly supervised.

2.2. Network Architectures in Vision Encoders

Vision encoders have evolved from Convolutional Neural Networks (CNNs), which leverage locality and translation equivariance for hierarchical feature learning but struggle with global dependencies due to fixed kernels [8, 14].

Vision Transformers (ViTs) tackled this issue by incorporating self-attention to image patches, achieving global receptive fields early on. This however has come with the cost of quadratic complexity in patch count and heavy data requirements [5].

SSMs have recently mitigated these trade-offs in computer vision. Models like Vision Mamba (ViM) [39] and its variants adapt bidirectional SSMs for linear-time processing of flattened image sequences, demonstrating strong performance in classification and beyond [19].

Hybrid approaches such as MambaVision [7] combine Mamba with Transformer elements for enhanced expressivity. Other variants, including VL-Mamba [25] for multimodal learning and GroupMamba [29] for vision tasks with efficient time and memory complexity, further expand the applicability of Mamba-based architectures.

Recent surveys [18, 37] highlight Mamba's growing adoption in new domains including remote sensing and image restoration, with scaling across resolutions. However, these models still treat images as static 1D sequences via raster scans, lacking dynamical, biologically inspired processing.

3. Method

3.1. Preliminaries

State Space Models. Our model is built upon a State Space Model (SSM) backbone. SSMs map a 1D input sequence $x(t)^{\perp}$ to an output y(t) through a latent state h(t), governed by a set of linear Ordinary Differential Equations (ODEs):

$$\frac{dh(t)}{dt} = \mathbf{A}h(t) + \mathbf{B}x(t) \tag{1}$$

$$y(t) = \mathbf{C}h(t) \tag{2}$$

where A, B, C are learned state matrices. This set of ODEs can be discretized using a timescale parameter Δ , yielding a recurrent formula:

$$h_t = \bar{\mathbf{A}}h_{t-1} + \bar{\mathbf{B}}x_t, \quad y_t = \mathbf{C}h_t \tag{3}$$

The Mamba architecture [3, 6] significantly advanced SSMs by introducing a selection mechanism that makes the model's parameters input-dependent, dramatically improving its ability to selectively process information. A key advantage of SSMs is their computational efficiency. During inference, they can operate as a recurrent system with constant memory per step; during training, it acts as a parallelizable convolutional system with linear-time complexity in sequence length.

Sequential Problem Formulation. Our work frames image classification as a sequential decision-making process. The model takes an input image $\mathbf{I} \in \mathbb{R}^{C \times H \times W}$, where C is the number of channels and H and W are the image height and width. The height and width are not constrained to a fixed size. From this image, it processes a sequence of inputs over T discrete time steps, $t \in \{0,...,T-1\}$. The model's final output is a sequence of classification logits $\mathbf{Y} \in \mathbb{R}^{T \times N}$, where N is the number of classes. Due to the model's causal nature, each vector $\mathbf{y}_t \in \mathbb{R}^N$ in the sequence represents the prediction after observing the first t inputs.

3.2. Data Processing

To create a model that mimics human-like visual processing, we reconsidered the standard data preprocessing pipeline. Our approach is based on sequential recognition, allowing the model's capabilities to be independent of a fixed input resolution. To implement this, we extract a sequence of $P \times P$ image patches from arbitrary coordinates, selected uniformly at random during training. This mirrors the saccadic movement of human eyes and contrasts with the fixed, non-overlapping grid used by ViTs [5].

To ensure robustness to various image resolutions, augmented images are not resized but are instead pasted onto the center of a larger, zero-padded canvas. For patch extraction, we sample from either exclusively from the original image region or from the entire canvas including the padding with equal probability. We also incorporate standard augmentation techniques such as random crops, perspective transformations, and color jittering to our training set.

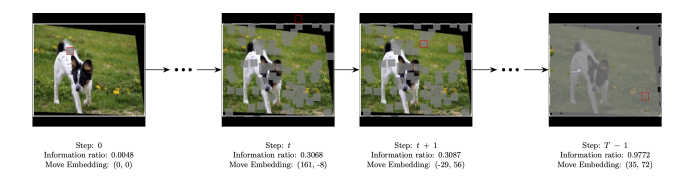


Figure 2. Illustration of the Sequential Data Processing Pipeline. The figure shows four snapshots of the data generation process. An original image is augmented and placed on a padded canvas (outlined by the white frame). At each step t, a new 16×16 patch (red border) is randomly sampled. The cumulative area covered by all patches is colored gray, and its proportion to the total image area defines the information ratio (r_t) . A move embedding, \mathbf{m}_t , is also computed from the relative coordinate shift from the previous patch, providing spatial context to the model.

For each step t, the model generates three key components as the input. This process is visualized in Figure 2:

- Image Patch Vector (\mathbf{v}_t) : A flattened $P \times P$ image patch, where $\mathbf{v}_t \in \mathbb{R}^{d_{\text{image}}}$ and $d_{\text{image}} = C \times P \times P$.
- Move Embedding (\mathbf{m}_t) : A sinusoidal position encoding of the relative coordinate change $(\Delta x, \Delta y)$ from the previous patch. The components are concatenated to form the move embedding, $\mathbf{m}_t \in \mathbb{R}^{d_{\text{move,emb}}}$. By encoding relative, rather than absolute positions, this approach provides a crucial inductive bias for translation invariance and is the key to the model's ability to operate on images of arbitrary shape and resolution. The initial embedding, \mathbf{m}_0 , is a zero vector.
- Information Ratio (r_t) : A scalar value, $r_t \in [0, 1]$, measuring the fraction of the image's unique area covered by the cumulative set of patches up to step t. This ratio is crucial for guiding the training loss.

¹In our model, the input sequence will be the sequence of image patches randomly extracted from the input image, which we will discuss later.

3.3. Model Architecture

MambaEye processes a sequence of image patches to perform classification. The architecture consists of three main components, as illustrated in Figure 3.

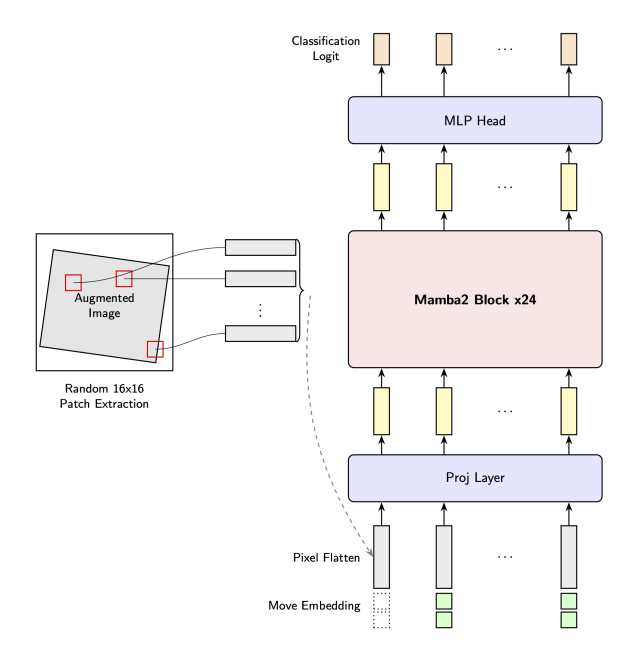


Figure 3. **MambaEye Model Architecture.** The diagram illustrates the sequential flow of the model. At each step, a flattened image patch vector and a sinusoidal "Move Embedding" are concatenated and processed by a projection layer. The core of the model is a stack of 24 Mamba2 blocks, whose output is passed to a final MLP head to produce a classification logit for that step.

Projection Head. At each step t, the image patch vector \mathbf{v}_t and the move embedding \mathbf{m}_t are concatenated to form an input vector $\mathbf{x}_t = [\mathbf{v}_t; \mathbf{m}_t] \in \mathbb{R}^{d_{\text{input}}}$, where $d_{\text{input}} = d_{\text{image}} + d_{\text{move_emb}}$. This vector is then projected into the model's hidden dimension, d_{model} , by a single-layer MLP, denoted f_{proj} , with a GELU activation [9].

$$\mathbf{z}_t^0 = f_{\text{proj}}(\mathbf{x}_t) \tag{4}$$

Mamba2 Backbone. The Mamba2 backbone is composed of L stacked blocks. Inherited from the underlying SSM, each block f_{mamba}^i supports dual inference modes. During training, it operates in a parallel mode, processing the entire sequence of embeddings \mathbf{Z}^i at once using an efficient convolutional representation:

$$\mathbf{Z}^{i+1} = f_{\text{mamba, parallel}}^{i}(\mathbf{Z}^{i}) \quad \text{for } i \in \{0, ..., L-1\}$$
 (5)

For inference, it can operate in a recurrent mode, processing one token at a time by updating a hidden state \mathbf{h}_t^i :

$$(\mathbf{z}_t^{i+1}, \mathbf{h}_t^{i+1}) = f_{\text{mamba, recurrent}}^i(\mathbf{z}_t^i, \mathbf{h}_{t-1}^{i+1}) \tag{6}$$

This recurrent formulation enables efficient, step-by-step processing with constant memory. Our choice of a unidirectional, causal flow—in contrast to the bidirectional approach often used in other vision backbones—is a deliberate design choice to preserve this structure, which is fundamental to our sequential framework.

Classification Head. Finally, each output representation \mathbf{z}_t^L from the backbone is passed through a single-layer MLP, the classification head f_{head} , to produce the classification logits for all N classes.

$$\mathbf{y}_t = f_{\text{head}}(\mathbf{z}_t^L) \tag{7}$$

This process yields the full sequence of predictions, $\mathbf{Y} = (\mathbf{y}_0, ..., \mathbf{y}_{T-1})$.

3.4. Diffusion-Inspired Loss Function

Our loss function is designed to train the model via a curriculum inspired by the iterative refinement process of diffusion models [2, 11] and flow matching models [17]. We frame classification as a sequential inference task, where the model's predictive distribution should evolve from a state of maximum uncertainty (a uniform prior) to one of complete certainty (the ground-truth label) as it gathers more visual information.

Let T be the sequence length and N be the number of classes. Let \mathbf{y}_t be the model's logit vector at step t. Let $\mathbf{p}_{\text{target}} \in \{0,1\}^N$ be the one-hot encoded ground-truth label, and let $\mathbf{p}_{\text{prior}} \in \mathbb{R}^N$ be a uniform distribution where each element is 1/N.

The schedule for this curriculum is governed by the information ratio, $r_t \in [0, 1]$. The scheduled target distribution at step t, denoted $\mathbf{p}_{\text{scheduled}}^{(t)}$, is defined as a linear interpolation:

$$\mathbf{p}_{\text{scheduled}}^{(t)} = (1 - r_t) \cdot \mathbf{p}_{\text{prior}} + r_t \cdot \mathbf{p}_{\text{target}}$$
(8)

The total loss \mathcal{L} is the mean Cross-Entropy (CE) loss computed over the entire sequence between the model's logits and the corresponding scheduled target:

$$\mathcal{L} = \frac{1}{T} \sum_{t=0}^{T-1} \text{CE}\left(\mathbf{p}_{\text{scheduled}}^{(t)}, \mathbf{y}_t\right)$$
(9)

where the CE loss for a single step is given by:

$$CE(\mathbf{p}, \mathbf{y}) = -\sum_{n=1}^{N} \mathbf{p}_n \log \left(\frac{\exp(\mathbf{y}_n)}{\sum_{i=1}^{N} \exp(\mathbf{y}_i)} \right)$$
(10)

This formulation provides dense supervision at every step, explicitly guiding the model to calibrate its confidence with the amount of visual evidence it has processed. By requiring an accurate prediction at every point along the schedule,

Table 1. Efficiency and scaling analysis of MambaEye. All metrics are measured on a single H100 GPU. Throughput and parallel memory are measured with a batch size of 128. Recurrent mode latency and memory are measured with a batch size of 1.

	FLOPs (G)		Throughput (img/s) [Parallel]		Latency (ms/step) [Recurrent]	Peak Memory (GB)			
Model	T = 1024	T = 4096	T = 1024	T = 4096	(Any T)	T = 1024 [Par.]	T = 4096 [Par.]	(Any T) [Rec.]	
MambaEye-T	11.71	46.84	4373.28	1124.99	6.88	3.11	12.21	0.06	
MambaEye-S	22.23	88.92	2229.14	573.84	13.22	3.13	12.23	0.08	
MambaEye-B	43.27	173.08	1130.29	290.37	21.88	3.17	12.27	0.13	

this loss also implicitly encourages the model's hidden state to act as a compressed summary of the visual information gathered, promoting efficient state management throughout the sequence.

4. Results

4.1. Implementation Details

Training Setup. We train our models from scratch for 300 epochs using the AdamW optimizer [20] with a total batch size of 1024. The learning rate follows a cosine decay schedule, warm up for 20 epochs to a peak of 1×10^{-3} before decaying to zero. We use optimizer betas of (0.9, 0.999) and a weight decay of 0.05.

Data Parameters. For data processing, we use a patch size of P=16, resulting in a patch vector dimension $d_{\rm image}=768$ (for 3-channel images). The move embedding has a dimension of $d_{\rm move_emb}=512$, with 256 dimensions allocated to each of the x and y coordinates. This yields a total input dimension $d_{\rm input}=1280$. During pre-training, the canvas size for each image is independently sampled from a uniform random distribution between 224^2 and 1024^2 resolution. The pre-training sequence length is set to T=1024.

Model Configurations. We experiment with three model sizes by varying the number of layers (L) while keeping the hidden dimension fixed to $d_{\rm model}=256$. Detailed configurations and model parameter sizes are tabulated at Table 2 below.

Table 2. Model Configurations

Model Config	Layers (L)	Parameters		
MambaEye-T (Tiny)	12	5.8M		
MambaEye-S (Small)	24	11.0M		
MambaEye-B (Base)	48	21.3M		

Fine-tuning. Following pre-training, we fine-tune the models on a longer sequence length of T=2048 for

30 epochs. For this stage, we follow the protocol of Vision Mamba [19], using a reduced constant learning rate of 1×10^{-5} and weight decay of 1×10^{-8} .

4.2. Computational Efficiency

We analyze the computational performance of our Mamba-Eye models, focusing on the key advantages of its architecture. As discussed in Section 3.3, our model supports dual inference modes: a parallel mode for high-throughput training and a recurrent mode for memory-efficient inference.

Table 1 provides a detailed scaling analysis of our three model sizes. We report theoretical FLOPs and practical inference metrics for both modes across different sequence lengths. All practical metrics (throughput, latency, memory) are measured on a single NVIDIA H100 GPU using FP32 precision. The total FLOPs are identical for both modes at a given sequence length T and FLOPs value is proportional to the sequence length. The recurrent mode's latency is reported per-step, and its memory footprint is constant, demonstrating the model's size-agnostic capability in memory complexity.

4.3. Training Results on ImageNet1K

We evaluate all model configurations (with and without fine-tuning) on the ImageNet-1K validation set across a wide range of image resolutions. For inference, images are resized to the target resolution while preserving their original aspect ratio, and then placed on a zero-padded canvas. Crucially, all patch sampling is constrained to the original image area, not the padding.

A unique feature of MambaEye is its ability to produce a prediction at any sequence length. As shown in Figure 4, we can analyze performance as a function of T. For most evaluations, we standardize our main results at a sequence length of T=4096, as model performance typically saturates before this point. While performance generally increases with longer sequences, we note an interesting anomaly in Figure 4(b): at low resolutions (e.g., 224^2 resolution), performance can degrade after a certain number of steps.

We present a series of controlled ablations to analyze our model's key characteristics, including the impact of our diffusion-inspired loss, the effect of image size, and the choice of scanning pattern.

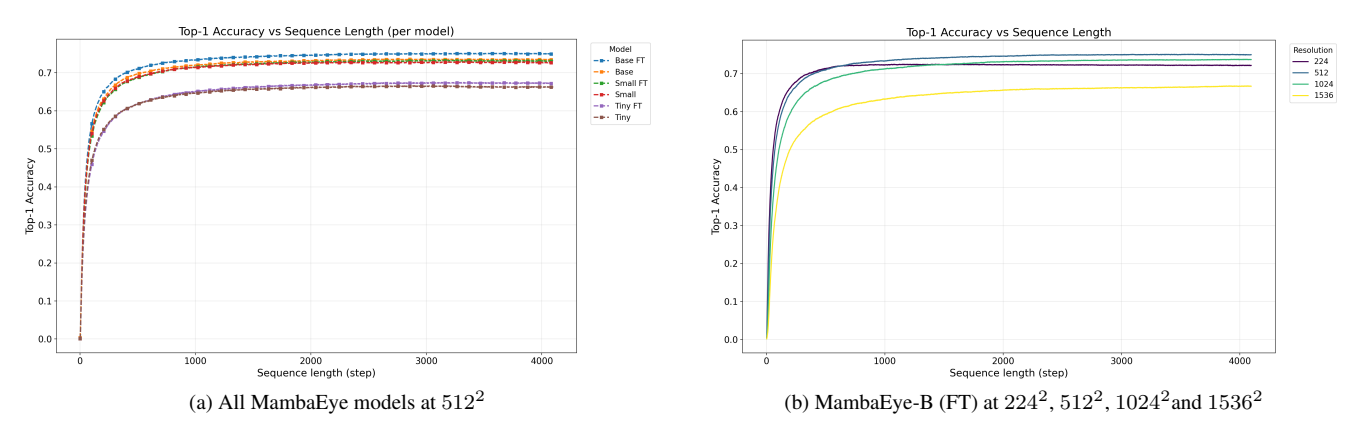


Figure 4. MambaEye performance vs. sequence length (T). (a) shows all model variants accumulating information at a fixed 512^2 resolution. Accuracy saturates for all models, with fine-tuned models achieving higher performance. (b) shows the MambaEye-B (FT) model across different resolutions, illustrating the trade-off between image size and required sequence length. At lower resolutions, performance saturates quickly, while higher resolutions require more steps.

Table 3. Top-1 Accuracy (%) on ImageNet-1K at various resolutions (T=4096). "FT" denotes models fine-tuned on T=2048 sequences. Competitor results are from Li et al. [15].

Model	224^{2}	256^{2}	384^{2}	512^{2}	640^{2}	768^{2}	1024^{2}	1280^{2}	1408^{2}	1536^{2}
MambaEye-T (5.8M)	61.1	62.9	65.8	66.2	66.2	65.3	63.3	60.6	58.8	56.5
MambaEye-T (FT) (5.8M)	62.1	63.7	66.7	67.2	67.1	66.4	64.4	61.6	59.8	57.4
MSVMamba (7M) [30]	77.3	77.7	77.4	75.0	71.7	65.8	48.0	31.0	23.8	18.3
ViM (7M) [39]	76.1	76.3	70.4	67.4	51.4	30.6	16.1	7.2	4.1	1.8
Efficient VMamba (6M) [23]	76.5	76.9	76.5	73.8	70.4	65.8	52.0	36.2	29.4	24.1
FractalMamba++ (7M) [15]	77.3	78.4	79.5	78.4	76.4	73.7	66.5	55.2	48.1	42.5
MambaEye-S (11M)	69.5	70.6	72.4	72.7	72.7	71.9	70.5	68.1	66.1	63.6
MambaEye-S (FT) (11M)	69.8	71.0	72.7	73.1	73.1	72.5	71.2	69.0	66.9	64.8
MSVMamba (12M) [30]	79.8 78.7 79.5	80.1	80.0	78.3	75.8	72.0	59.4	43.9	36.5	29.9
Efficient VMamba (11M) [23]		79.6	79.5	77.3	75.2	72.4	64.2	54.1	42.6	38.3
FractalMamba++ (11M) [15]		80.6	82.0	81.3	80.1	78.3	73.3	66.3	61.7	56.1
MambaEye-B (21M)	70.6	71.7	73.3	73.5	73.4	72.9	71.7	69.4	67.0	64.3
MambaEye-B (FT) (21M)	72.2	73.2	74.8	75.0	75.0	74.6	73.7	71.5	69.5	66.7
VMamba (31M) [39]	82.5	82.5	82.5	81.1	79.3	76.1	62.3	50.2	45.1	40.9
FractalMamba++ (30M) [15]	83.0	83.5	84.1	83.9	83.0	81.9	78.8	74.3	71.3	67.5

4.3.1. Loss Function Ablation

To validate the effect of our proposed diffusion-inspired loss, we compare the two models with both using the MambaEye-T architecture, and without fine-tuning process, evaluated at T=4096. For comparison, one of the models is trained with a standard cross entropy (CE) loss, applied to the output logit of every sequence, $\mathbf{y}_t, t \in \{0,...,T-1\}$, while the other utilizes our new diffusion-based loss.

Table 4 demonstrates that our new loss function has a demonstrable impact on the performance. The baseline model trained with a standard cross entropy loss achieves

a lower top-1 accuracy in every resolution.

This result strongly validates our core hypothesis: for a sequential processing model, dense, step-wise supervision is beneficial. The standard cross entropy loss is less optimized in providing sufficient training signals for the model to learn how to effectively cumulate and refine information over time. Our diffusion-inspired loss provides a clear framework, teaching the model to build a progressively more accurate prediction as it gathers more visual evidence. More details are provided in the Supplementary Material.

Table 4. Ablation study of the loss function on ImageNet-1K.

Loss Function	224^{2}	512^{2}	1024^{2}	1536^{2}
Standard CE	56.7	61.9	59.9	53.6
Ours (Diffusion-inspired)	61.1	66.2	63.3	56.5

4.3.2. Ablation on Image Size

A key claim of our work is that MambaEye's architecture is size-agnostic. To test this, we evaluate our pretrained models, with and without long-sequence fine-tuning, on a wide range of image resolutions from 224^2 to 1536^2 . For each evaluation, the model processes a sequence of T=4096 randomly sampled patches. The results are shown in Table 3. We compare our models against recent Mamba-based backbones designed for resolution scaling.

Across Tiny, Small, and Base, accuracy tends to peak around mid resolutions (roughly 384^2 – 640^2) and then softens as resolution continues to grow. This is consistent with the fixed sequence budget: with T=4096, higher resolutions dilute the coverage per step, so the model needs more steps to get full information from the image. Scaling to larger models help consistently, the fine-tuned variants of Tiny/Small/Base reach 67.2/73.1/75.0 at 512^2 . The advantage of scaling persists even at 1536^2 , with 57.4/64.8/66.7 top-1 accuracy, but the overall shape of the curve remains similar. Fine-tuning also plays a clear role. It increases accuracy across the board and makes the high resolution tail more resilient (e.g., at 1536^2 , +0.9/+1.2/+2.4 points for Tiny/Small/Base).

The high resolution behavior is remarkably uniform across model sizes: the absolute drop from the peak to 1536^2 is on the order of 8–10 points for all three scales (e.g., Small (FT) $73.1 \rightarrow 64.8$ and Base (FT) $75.0 \rightarrow 66.7$).

At low and mid resolutions, methods like Fractal-Mamba++ typically attain higher peaks at similar parameter counts. However, as we move into the high-resolution regime, the gap narrows or reverses for smaller models: at 1280^2 to 1536^2 , our Tiny and Small (FT) variants surpass size-matched baselines, and the Base (FT, 21M) model closes on 30–31M-parameter alternatives. This aligns with our central claim. Even with a naive random sampling policy, the architecture scales robustly with resolution.

4.3.3. Ablation on Scanning Patterns

To understand the impact of the scanning policy, we evaluated deterministic scanning patterns (horizontal raster and horizontal zigzag) across multiple image sizes with MambaEye-B (FT).

For this experiment, we first split the image into a grid of non-overlapping 16×16 patches. Similar to our random sampling setup, we preserved the original image's aspect ratio on a canvas and only extracted patches from the valid

image area. These patches were then fed to the model using fixed, deterministic scanning patterns: a horizontal raster sweep and a horizontal zigzag sweep. As with other ablations, we used a fixed sequence length of T=4096. If the total number of patches in the grid was less than 4096 (e.g., for resolutions below 1024^2), the sequence was repeated from the start to fill the context. Conversely, for resolutions above 1024^2 , the model did not see all patches in the image within the 4096-step budget.

The results, shown in Table 5, are striking. Compared to the accuracy from random sampling, the deterministic scanning is incompatible with our architecture. While already not ideal at lower resolutions, the performance degrades rapidly at higher resolutions where our random sampling protocol excels. This result highlights the difference between other Mamba-based models and our unidirectional model which is inherently adaptable to arbitrary scanning patterns and performance can be varied. The two deterministic patterns exhibit similar overall performance.

Figure 5 provides insight for the incomptibility of our model training with the raster and zigzag scans. Under the horizontal raster scan, top-1 accuracy oscillates at both high and low frequencies as the sequence progresses. We hypothesize that the high frequency oscillations occur at row changes because the scan wraps to the first pixel of the next row, inducing a large horizontal jump that disrupts the model's causal state; the low-frequency oscillations correspond to full sequence repetitions. By contrast, the horizontal zigzag scan continues left-to-right then right-to-left, so at a row change it moves down by only one pixel and proceeds from the adjacent column. This removes most high-frequency oscillations; instead, we observe small steplike drops aligned with row transitions. Both plots support this hypothesis. Overall, simple deterministic scans are a poor fit for our model: despite the architecture's flexibility, it struggles to maintain context after the spatially incoherent moves inherent in raster-style patterns. This strongly isolates the scanning policy as a critical component for performance. Additionally, these results suggest that there may exist superior scanning policies compared to random patch extraction, such as adaptive scanning paths tailored to each individual image.

Table 5. Ablation study on fixed scanning patterns.

Scanning Pattern	224^{2}	512^{2}	1024^{2}	1536^{2}
Random	72.2	75.0	73.7	66.7
Horizontal Raster Scan	45.3	38.9	12.5	6.0
Horizontal Zigzag Scan	50.2	34.8	16.7	6.4

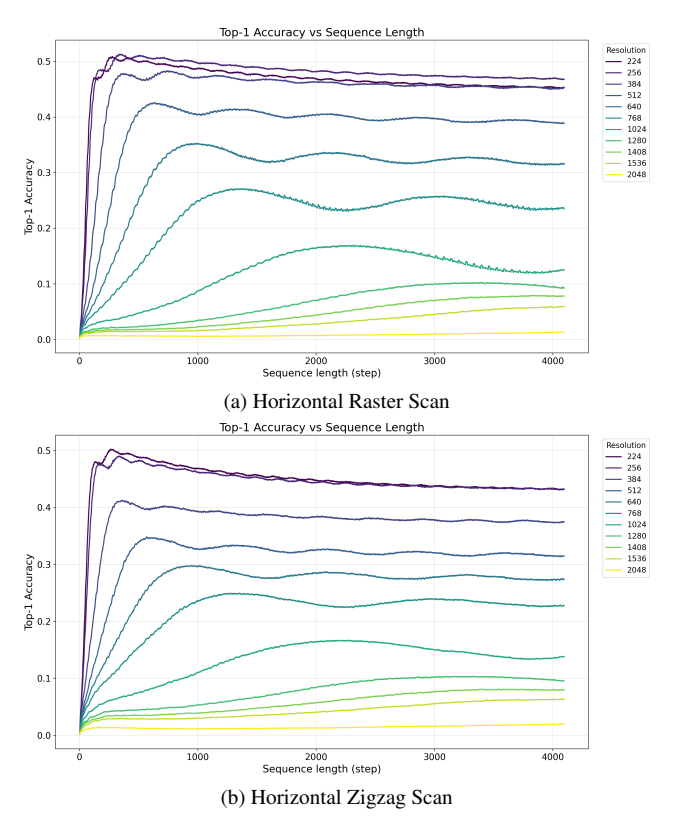


Figure 5. Deterministic scanning patterns: performance vs. sequence length. Top-1 accuracy of the MambaEye-B (FT) model under horizontal raster and horizontal zigzag scans, plotted over the sequence length (T=4096) for multiple resolutions. For the raster scan, wrapping to the first pixel of the next row causes large horizontal jumps and pronounced high-frequency oscillations; for the zigzag scan, the inter-row transition is a 1-pixel vertical move with adjacent horizontal continuity, suppressing high-frequency oscillations but this method still performs substantially worse compared to random sampling.

5. Conclusion

In this work, we introduced **MambaEye**, a novel visual encoder that re-frames image recognition as a causal, sequential-processing task. Our approach is built on a pure Mamba2 backbone, preserving its linear-time efficiency and constant-memory inference. We presented two core innovations: a **relative move embedding** that provides translation invariance for arbitrary scanning paths, and a **diffusion-inspired loss function** that provides dense, step-wise supervision.

Our experimental results validate this new paradigm. We demonstrated that our diffusion-inspired loss is critical, improving performance compared to a standard cross entorpy loss (Table 4). We also proved that our architecture's flexibility is genuine. The model's performance with a simple random scan dramatically exceeds deterministic scanning

patterns (Table 5), confirming that the relative move embedding successfully provides spatial context.

While our model's peak accuracy does not yet match architectures with deterministic scanning path, at lower resolutions, we show that its performance scaling is highly robust, outperforming pervious Mamba based encoders for small and intermediate sized models.

Limitations and future work While MambaEye is promising, we identify several limitations that guide future work. Our current training omits advanced augmentations like CutMix [35] or Mixup [36], and our architectural study is limited. A further ablation on image augmentation and bringing up the performance for larger model parameters will also be helpul. In a more bird's eye view, it will be worth it to understand MambaEye's unidirectional architecture and its general compatibility with other complex structures like H-Net [12] could yield further improvements. A key future direction is a systematic study of generalization, not only to longer sequences [27] but also to higher dimensional data like video or 3D volumes, which could be supported by adapting the move embedding with higher dimension. Finally, the most significant future step is to replace random patch sampling with a learned, adaptive scanning policy, bringing the model's efficiency closer to that of human vision.

References

- [1] J Ba, V Mnih, and K Kavukcuoglu. Multiple object recognition with visual attention. arxiv 2014. arXiv preprint arXiv:1412.7755, 2014. 2
- [2] Arpit Bansal, Eitan Borgnia, Hong-Min Chu, Jie Li, Hamid Kazemi, Furong Huang, Micah Goldblum, Jonas Geiping, and Tom Goldstein. Cold diffusion: Inverting arbitrary image transforms without noise. Advances in Neural Information Processing Systems, 36:41259–41282, 2023. 2, 4
- [3] Tri Dao and Albert Gu. Transformers are ssms: Generalized models and efficient algorithms through structured state space duality. arXiv preprint arXiv:2405.21060, 2024. 2, 3
- [4] Luke Darlow, Ciaran Regan, Sebastian Risi, Jeffrey Seely, and Llion Jones. Continuous thought machines. arXiv preprint arXiv:2505.05522, 2025. 2
- [5] Alexey Dosovitskiy, Lucas Beyer, Alexander Kolesnikov, Dirk Weissenborn, Xiaohua Zhai, Thomas Unterthiner, Mostafa Dehghani, Matthias Minderer, Georg Heigold, Sylvain Gelly, et al. An image is worth 16x16 words: Transformers for image recognition at scale. arXiv preprint arXiv:2010.11929, 2020. 1, 2, 3
- [6] Albert Gu and Tri Dao. Mamba: Linear-time sequence modeling with selective state spaces. In *First Conference on Language Modeling*, 2024. 1, 3
- [7] Ali Hatamizadeh and Jan Kautz. Mambavision: A hybrid mamba-transformer vision backbone. In *Proceedings of the Computer Vision and Pattern Recognition Conference*, pages 25261–25270, 2025. 2

- [8] Kaiming He, Xiangyu Zhang, Shaoqing Ren, and Jian Sun. Deep residual learning for image recognition. In *Proceedings of the IEEE conference on computer vision and pattern recognition*, pages 770–778, 2016. 1, 2
- [9] Dan Hendrycks and Kevin Gimpel. Gaussian error linear units (gelus). arXiv preprint arXiv:1606.08415, 2016. 4
- [10] Byeongho Heo, Song Park, Dongyoon Han, and Sangdoo Yun. Rotary position embedding for vision transformer. In European Conference on Computer Vision, 2024.
- [11] Jonathan Ho, Ajay Jain, and Pieter Abbeel. Denoising diffusion probabilistic models. *Advances in neural information processing systems*, 33:6840–6851, 2020. 2, 4
- [12] Sukjun Hwang, Brandon Wang, and Albert Gu. Dynamic chunking for end-to-end hierarchical sequence modeling. arXiv preprint arXiv:2507.07955, 2025. 8
- [13] Fady Ibrahim, Guangjun Liu, and Guanghui Wang. A survey on mamba architecture for vision applications. arXiv preprint arXiv:2502.07161, 2025. 2
- [14] Yann LeCun, Léon Bottou, Yoshua Bengio, and Patrick Haffner. Gradient-based learning applied to document recognition. *Proceedings of the IEEE*, 86(11):2278–2324, 2002.
- [15] Bo Li, Haoke Xiao, and Lv Tang. Scaling vision mamba across resolutions via fractal traversal. arXiv preprint arXiv:2505.14062, 2025. 1, 2, 6
- [16] Yuan Li et al. Polaformer: A polarity-aware linear attention for vision transformers. In arXiv preprint arXiv:2501.15061, 2025.
- [17] Yaron Lipman, Ricky TQ Chen, Heli Ben-Hamu, Maximilian Nickel, and Matt Le. Flow matching for generative modeling. In 11th International Conference on Learning Representations, ICLR 2023, 2023. 2, 4
- [18] Xiao Liu, Chenxu Zhang, and Lei Zhang. Vision mamba: A comprehensive survey and taxonomy. *arXiv preprint arXiv:2405.04404*, 2024. 3
- [19] Yue Liu, Yunjie Tian, Yuzhong Zhao, Hongtian Yu, Lingxi Xie, Yaowei Wang, Qixiang Ye, Jianbin Jiao, and Yunfan Liu. Vmamba: Visual state space model. *Advances in neural* information processing systems, 37:103031–103063, 2024. 2, 5
- [20] Ilya Loshchilov and Frank Hutter. Decoupled weight decay regularization. arXiv preprint arXiv:1711.05101, 2017. 5
- [21] Volodymyr Mnih, Nicolas Heess, Alex Graves, and Koray Kavukcuoglu. Recurrent models of visual attention. *Advances in neural information processing systems*, 27, 2014.
- [22] Thomas Parr, Noor Sajid, Lancelot Da Costa, M Berk Mirza, and Karl J Friston. Generative models for active vision. *Frontiers in Neurorobotics*, 15:651432, 2021. 2
- [23] Xiaohuan Pei, Tao Huang, and Chang Xu. Efficientvmamba: Atrous selective scan for light weight visual mamba. In *Proceedings of the AAAI Conference on Artificial Intelligence*, pages 6443–6451, 2025. 6
- [24] Nedyalko Prisadnikov, Danda Pani Paudel, Yuqian Fu, and Luc Van Gool. Vision encoders should be image size agnostic and task driven. *arXiv preprint arXiv:2508.16317*, 2025.

- [25] Yanyuan Qiao, Zheng Yu, Longteng Guo, Sihan Chen, Zijia Zhao, Mingzhen Sun, Qi Wu, and Jing Liu. Vl-mamba: Exploring state space models for multimodal learning. arXiv preprint arXiv:2403.13600, 2024. 3
- [26] Laura Walker Renninger, James Coughlan, Preeti Verghese, and Jitendra Malik. An information maximization model of eye movements. Advances in Neural Information Processing Systems, 17, 2005.
- [27] Ricardo Buitrago Ruiz and Albert Gu. Understanding and improving length generalization in recurrent models. arXiv preprint arXiv:2507.02782, 2025. 8
- [28] Olga Russakovsky, Jia Deng, Hao Su, Jonathan Krause, Sanjeev Satheesh, Sean Ma, Zhiheng Huang, Andrej Karpathy, Aditya Khosla, Michael Bernstein, Alexander C. Berg, and Li Fei-Fei. ImageNet Large Scale Visual Recognition Challenge. *International Journal of Computer Vision (IJCV)*, 115 (3):211–252, 2015. 2
- [29] Abdelrahman Shaker, Syed Talal Wasim, Salman Khan, Juergen Gall, and Fahad Shahbaz Khan. Groupmamba: Efficient group-based visual state space model. In *Proceedings* of the Computer Vision and Pattern Recognition Conference, pages 14912–14922, 2025. 3
- [30] Yuheng Shi, Minjing Dong, and Chang Xu. Multi-scale vmamba: Hierarchy in hierarchy visual state space model. Advances in Neural Information Processing Systems, 37: 25687–25708, 2024. 6
- [31] Jianlin Su, Yu Lu, Shengfeng Pan, Ahmed Murtadha, Bo Wen, and Yunfeng Liu. Roformer: Enhanced transformer with rotary position embedding. In *Proceedings of the 32nd International Conference on Neural Information Processing Systems*, 2021. 1
- [32] Hugo Touvron, Andrea Vedaldi, Matthijs Douze, and Hervé Jégou. Fixing the train-test resolution discrepancy. In *Advances in Neural Information Processing Systems*, 2019. 1
- [33] Haoke Xiao, Lv Tang, Peng-tao Jiang, Hao Zhang, Jinwei Chen, and Bo Li. Boosting vision state space model with fractal scanning. In *Proceedings of the AAAI Conference on Artificial Intelligence*, pages 8646–8654, 2025. 2
- [34] Zhaodong Yang et al. Rank-augmented linear attention for efficient vision transformers. In *Proceedings of the IEEE/CVF Conference on Computer Vision and Pattern Recognition*, 2025. 1
- [35] Sangdoo Yun, Dongyoon Han, Seong Joon Oh, Sanghyuk Chun, Junsuk Choe, and Youngjoon Yoo. Cutmix: Regularization strategy to train strong classifiers with localizable features. In *Proceedings of the IEEE/CVF international con*ference on computer vision, pages 6023–6032, 2019. 8
- [36] Hongyi Zhang, Moustapha Cisse, Yann N Dauphin, and David Lopez-Paz. mixup: Beyond empirical risk minimization. In *International Conference on Learning Representa*tions, 2018. 8
- [37] Hanwei Zhang, Ying Zhu, Dan Wang, Lijun Zhang, Tianxiang Chen, and Zi Ye. A survey on visual mamba. *arXiv* preprint arXiv:2404.15956, 2024. 3
- [38] Qi Zhang et al. Focused linear attention for high-efficiency vision transformers. In Proceedings of the IEEE/CVF International Conference on Computer Vision, pages 5533–5543, 2023.

[39] Lianghui Zhu, Bencheng Liao, Qian Zhang, Xinlong Wang, Wenyu Liu, and Xinggang Wang. Vision mamba: efficient visual representation learning with bidirectional state space model. In *Proceedings of the 41st International Conference on Machine Learning*, pages 62429–62442, 2024. 2, 6